Published in final edited form as:
J Nucl Med. 2010 January ; 51(1): 37–45. doi:10.2967/jnumed.109.067009.

Pharmacokinetic Analysis of Hypoxia ^{18}F-Fluoromisonidazole Dynamic PET in Head and Neck Cancer

Wenli Wang[1], **Nancy Y. Lee**[2], **Jens-Christoph Georgi**[3], **Manoj Narayanan**[4], **Jose Guillem**[5], **Heiko Schöder**[6], and **John L. Humm**[1]

[1] Department of Medical Physics, Memorial Sloan-Kettering Cancer Center, New York, New York

[2] Department of Radiation Oncology, Memorial Sloan-Kettering Cancer Center, New York, New York

[3] Philips Technologie GmbH Forschungslaboratorien, Molecular Imaging Systems, Aachen, Germany

[4] Philips Research North America, Briarcliff Manor, New York

[5] Department of Surgery, Memorial Sloan-Kettering Cancer Center, New York, New York

[6] Department of Radiology, Memorial Sloan-Kettering Cancer Center, New York, New York

Abstract

This study used pharmacokinetic analysis of ^{18}F-labeled fluoromisonidazole (^{18}F-FMISO) dynamic PET to assist the identification of regional tumor hypoxia and to investigate the relationship among a potential tumor hypoxia index (K_i), tumor-to-blood ratio (T/B) in the late-time image, plasma-to-tissue transport rate (k_1), and local vascular volume fraction (β) for head and neck cancer patients.

Methods—Newly diagnosed patients underwent a dynamic ^{18}F-FMISO PET scan before chemotherapy or radiotherapy. The data were acquired in 3 consecutive PET/CT dynamic scan segments, registered with each other and analyzed using pharmacokinetics software. The (K_i, k_1, β) kinetic parameter images were derived for each patient.

Results—Nine patients' data were analyzed. Representative images of ^{18}F-FDG PET (of the tumor), CT (of the anatomy), and late-time ^{18}F-FMISO PET (of the T/B) and parametric images of K_i (potentially representing tumor hypoxia) are shown. The patient image data could be classified into 3 types: with good concordance between the parametric hypoxia map K_i and high T/B, with concordant findings between the parametric hypoxia map and low T/B, and with ambiguity between parametric hypoxia map and T/B. Correlation coefficients are computed between each pair of T/B, K_i, k_1, and β. Data are also presented for other potential hypoxia surrogate measures, for example, k_3 and k_1/k_2.

Conclusion—There is a positive correlation of 0.86 between the average T/B and average hypoxia index K_i of the region of interest. However, because of the statistical photon counting noise in PET and the amplification of noise in kinetic analysis, the direct correlation between the T/B and hypoxia of the individual pixel is not obvious. For a tumor region of interest, there is a slight negative correlation between k_1 and K_i, moderate positive correlation between β and K_i, but no correlation between β and k_1.

For correspondence or reprints contact: John Humm, Department of Medical Physics, Memorial Sloan-Kettering Cancer Center, 1275 York Ave., New York, NY 10021. hummj@mskcc.org.

Keywords

hypoxia; head and neck cancer; PET; ^{18}F-FMISO; pharmacokinetics

Hypoxia is known as a prognostic factor for many types of cancer, for example, cervical cancer (1), sarcoma (2), and prostate cancer (3). For locally advanced squamous cell carcinoma of the head and neck, tumor hypoxia has been reported to be an important determinant of treatment failure (4–7).

The direct measurement of tumor partial oxygen pressure (pO_2) can be made using the Eppendorf electrode (Eppendorf AG) or OxyLite probe (Oxford Optronics). With these methods, tumor hypoxia is usually identified as pO_2 values less than or equal to 10 mm Hg. However, pO_2 probe measurement is invasive and may result in sampling error because of the limited number of points that can be feasibly obtained, limited accessibility with some tumors, and an inability to distinguish hypoxic tumor from necrotic tissue. Another method for studying tumor hypoxia is immunohistochemical analysis. However, this method depends on the availability of tumor specimens and again may result in sampling errors associated with the small fraction of tissue analyzed.

PET is a noninvasive approach to image function, such as metabolism, proliferation, blood flow, and hypoxia. PET provides a 3-dimensional quantitative image of the whole tumor, is repeatable during treatment, and may distinguish viable hypoxic tumor from a nonviable necrotic area. Multiple radiotracers have been developed for the purpose of hypoxia imaging: for example, ^{18}F-labeled fluoromisonidazole (^{18}F-FMISO) (8–11). The drug diffuses into and out of the cell in the presence of oxygen but mostly becomes irreversibly bound to macromolecules in the cell under hypoxic conditions (12,13). Although part of the hypoxic binding of the drug is reversible, this effect is small and thus is ignored in this article.

Previous clinical studies on static ^{18}F-FMISO PET for head and neck cancer patients were performed at the University of Washington. Analysis of the ^{18}F-FMISO image 90–140 min after injection led to an operational definition of tumor hypoxia corresponding to a tumor-to-blood activity concentration ratio of greater than 1.2–1.6 (9,14,15). However, the physiologic clearance of ^{18}F-FMISO from highly perfused normal tissue may result in the same tumor-to-blood ratio (T/B), which is comparable to hypoxic tumor at the time of patient imaging. At 90–180 min after injection, the activity concentration in normal tissue continually decreases as a function of time, whereas in hypoxic tumor it increases as a function of time. The possibility of a cross-over point between the decline in activity from a well-perfused tissue region and the increasing activity from a predominantly hypoxic one can result in an ambiguity in the interpretation of single-time-point imaging.

Therefore, we investigated a kinetic approach, to compare with imaging at a single late time point for identifying regional tumor hypoxia. For this purpose, ^{18}F-FMISO data were obtained using a dynamic acquisition protocol for use in pharmacokinetic compartmental modeling. The compartmental analysis tool we used was based on a generic 2-tissue model implemented in Philips Voxulus software. Prior investigations using this generic tool for dynamic ^{18}F-FMISO PET data have been published by Thorwarth et al. (16) and applied for head and neck cancer patients (17). To test the accuracy and precision of this voxelwise approach to compartmental modeling, we used a mathematic dynamic phantom to simulate the ^{18}F-FMISO kinetics based on predefined compartmental transfer rate constants, initially with no statistical noise (to verify accuracy) and then with gaussian noise comparable to the clinical PET data observed in our patient study group (to verify precision). The results of this simulation study and the impact

of the accuracy of the compartmental model by the shift error in the plasma input function are reported by Wang et al. (18).

The aim of this study was to investigate the correlation between 2 potential parametric measures of hypoxia, k_3 and K_i, and T/B in a late-time ^{18}F-FMISO image; plasma-to-tissue transport rate as a surrogate for local blood perfusion; and local vascular volume fraction in pretreatment patients with head and neck cancer.

MATERIALS AND METHODS

Patient Selection and Imaging Protocol

Nine newly diagnosed patients with local squamous cell carcinoma head and neck cancers with no prior chemotherapy or radiotherapy were included in this study. There were 8 men and 1 woman (age range, 50–66 y). The disease stage ranged from I to IV for tumors and I to III for lymph node involvement but without distant metastasis. All patients underwent routine whole-body ^{18}F-FDG PET/CT to identify the sites of disease. Within 1–3 d, a dynamic ^{18}F-FMISO PET/CT scan was performed. The ^{18}F-FMISO imaging protocol was approved by Memorial Sloan-Kettering Cancer Center's Institutional Review Board (IRB 04-070) originally in 2004 and subsequently amended to perform dynamic PET in 2007. All patients were required to provide written informed consent.

^{18}F-FMISO PET/CT Data Acquisition and Processing

The PET/CT data were acquired on the GE Discovery STE in 2-dimensional mode. Patients were placed supine and fastened with a head-and-shoulder immobilization mask, in the radiotherapy treatment position. A low-dose CT scan (140 kVp, 10 mA) was acquired, with the tumor positioned in the center of a single 15-cm axial field of view. The patient was injected intravenously with 370 MBq of ^{18}F-FMISO as a bolus, simultaneous with the start of the dynamic PET scan acquisition. The dynamic PET data were acquired in 1-min time frames continuously from 0 to 5 min and in 5-min time frames continuously from 5 to 30 min. The patient was then removed from the scanner and instructed to return at 90 min for a second PET/CT scan and again at 180 min for a third scan. The second and third scans were acquired first with the same low-dose CT, followed by a dynamic PET scan in two 5-min time frames. These 3 low-dose CT scans were used for both PET attenuation correction and registration of 3 series of PET images. The PET data were reconstructed using Fourier rebinning and a 2-dimensional ordered-subset expectation maximization algorithm with attenuation and scatter corrections into 14 dynamic frames (128 × 128 × 47, with 4.69-mm transverse pixel size and 3.27-mm axial pixel size). A local coregistration technique as implemented in Pinnacle (Phillips) was used to derive the rigid transformation matrix from the second and third CT scans with respect to the first one, which was then applied to the second and third sets of dynamic PET data to generate a registered dynamic series for pharmacokinetic analysis.

Pharmacokinetic Analysis

The Philips Voxulus software package, which is also included in the research version of Philips' radiation treatment planning software Pinnacle and preclinical software package Imalytics, was used for pharmacokinetic analysis. In pharmacokinetic analysis, the time-varying activity concentration can be partitioned into 3 compartments (19): $C_p(t)$, $C_1(t)$, and $C_2(t)$, as shown in Figure 1. This partition is only conceptual, not physical. The $C_p(t)$, $C_1(t)$, and $C_2(t)$ are the activity concentration (units are Bq/mL) as a function of time t (unit in min) after injection in the plasma compartment, reversible tissue compartment, and trapped tissue compartment, respectively; and k_1, k_2, and k_3 are the kinetic reaction rate constants (in units of 1/min) between compartments. The rate constants k_1 and k_2 represent the ^{18}F-FMISO transport rate from the plasma compartment to the reversible tissue compartment and the diffusion rate out of the

reversible tissue compartment. At early times, k_1 can be used as a surrogate for blood perfusion when the extraction is close to unity. The k_3 indicates the ^{18}F-FMISO retention rate constant, from the reversible to the trapped compartment, and is a potential surrogate measure of hypoxia. Another more direct and stable surrogate measure of hypoxia may be the influx rate constant $K_i = \frac{k_1 k_3}{k_2 + k_3}$ (18). K_i indicates the direct retention rate constant from the plasma compartment to the trapped compartment without going through the reversible compartment. At late times, if the plasma compartment contribution approaches zero, the activity concentration is proportional to K_i. The selection of a plasma input function is a requisite step in pharmacokinetic analysis. The plasma input function can be obtained from the arterial blood sampling or from an arterial blood region in the PET images. The plasma compartment in each voxel is only a fraction of the plasma input function. Thus, a vascular volume fraction β (a scale from 0 to 1), compared with the plasma input function, is used to indicate the ratio of vascular volume in tissue at each voxel. For a multiple-voxel tumor region, Voxulus was able to estimate each kinetic parameter as a kinetic image of voxels within the region.

Image-Based Plasma Input Function

In this study, we used an image-based plasma input function (20–22) instead of blood sampling. The input function region was selected on the common carotid artery from the summed dynamic image at the first 3 min after injection. The diameter of the common carotid artery for a 55-y-old population is about 6.3 ± 0.6 mm for men and 5.6 ± 0.5 mm for women (23), which is about 1–2 voxels in a PET image. About 20 voxels with highest image intensity in the coronal view of the common carotid artery region were selected for the input function, without correction for the partial-volume effects. The measured input function was then fitted with an analytic formula to capture the correct shape of the input function. The coarse initial frame duration of 1 min was selected to provide adequate statistics when performing voxel-by-voxel compartmental analysis. Simulation studies have been conducted to examine the impact of the sharpness of the input function peak and the effect of image noise on the estimation of the rate constants k_1, k_2, k_3, β, and K_i, and that work has been published separately (18).

Region-of-Interest (ROI) Definition and Analysis

Each patient's tumor ROI was defined on the patient's ^{18}F-FDG PET image with a standardized uptake value greater than 50% of local maximum standardized uptake value, independent of the ^{18}F-FMISO late-time image or kinetic parametric image. This ROI was then used to derive the average kinetic parameters and other tumor-related statistics from the patient's ^{18}F-FMISO PET images. The last 10-min time frame of the ^{18}F-FMISO PET, corresponding to approximately 3 h after injection, was used as the late-time image. The T/B was defined as the ratio of average activity concentration in the tumor ROI versus the plasma input function region at late time. The tumor noise at the late-time imaging was defined as the SD of the voxel intensities within the tumor ROI versus its mean.

Scatter Plot and Pearson Correlation Coefficient

Scatter plots were used as a method to visualize the relationship between 2 kinetic parameters of interest for a set of data points corresponding to tumor ROI or to the whole image space. The Pearson correlation coefficient was computed between 2 kinetic parameters to indicate the strength and direction of a linear relationship between these 2 parameters.

RESULTS

Table 1 shows the summary of the pharmacokinetic analysis of the 9 head and neck cancer patients. Patients 1–3 have estimated values for the tumor ROI hypoxia index K_i greater than

0.003 (1/min), whereas the rest of the patients have K_i less than 0.003 (1/min), suggesting lower hypoxic volumes within patients 4 through 9.

Correlation of Tumor Hypoxia and T/B at Late Time

For patients 1–9, the correlation coefficients for individual voxels within the tumor ROI of ^{18}F-FMISO T/B at a late time and K_i were 0.46, 0.24, 0.07, 0.10, 0.34, −0.14, 0.30, 0.12, and 0.40. The coefficients for individual voxels suggest that there is no consistent correlation between T/B and K_i for individual voxels within the tumor ROI. Most of the variation of the T/B and K_i in the ROI could be due to the statistical noise present in the PET data measurement and propagated through the image reconstruction and pharmacokinetic parameter estimation. Figure 2 displays the scatter plot of the average T/B versus K_i over the tumor ROI, with each plus sign corresponding to a patient whose number is indicated next to it. In this scatter plot, T/B and K_i are positively correlated, with a correlation coefficient of 0.86. The dashed line indicates the linear regression between these 2 parameters, where $K_i = 0.00325 \times \text{T/B} - 0.00286$.

Figure 3 shows the images from patient 2, who exhibited a good concordance between the regions of high T/B in the late-time image and the parametric K_i image believed to be representative of hypoxia. Figure 3A displays the transverse, coronal, and sagittal views of ^{18}F-FDG PET, ^{18}F-FMISO PET at a late time, CT, and the parametric images k_1, K_i, and β. The tumor ROI is shown in the CT images. Both the late-time ^{18}F-FMISO PET image and the K_i image (a hypoxia measure) had high voxel intensities in this ROI, and the K_i image had higher tumor-to-background contrast than the late-time ^{18}F-FMISO image. The surrogate perfusion rate constant k_1 image had low voxel intensity in this ROI. There was no clear trend of voxel intensity in the vascular volume fraction β in this ROI, because part of the ROI was close to the common carotid artery. Figure 3B displays the measured and fitted average activity concentration in the tumor ROI as a function of time. Both curves had an early peak at 1–2 min and then decayed and reached a minimum at 20 min; then both curves gradually increased at a later time because more ^{18}F-FMISO was trapped in the tumor ROI. The estimated average kinetic parameters are also shown in the plot, with $k_1 = 0.06$ (1/min), $K_i = 0.0042$ (1/min), β = 0.25, and the average T/B at a late time = 1.74.

Figure 4 shows images from patient 9 and represents a negative finding for hypoxia by PET. This case shows a good concordance between the general low T/B in a late-time image and the corresponding low K_i values. At the tumor ROI, shown in the CT image in Figure 4A, the average T/B in the late-time image is 1.19, which is not high compared with other regions in the late-time image. The average K_i in tumor ROI is 0.0009 (1/min), which is in the medium range, compared with other regions. The average k_1 in the tumor ROI is 0.26 (1/min), which is slightly higher than other regions. The average β in the tumor ROI is 0.10, which is also in the medium range, compared with other regions. The tumor ROI time–activity curve, as shown in Figure 4B, had an early peak at 1–2 min similar to that for patient 2, but kept decreasing at a late time, which was different from patient 2 and suggested little trapping of ^{18}F-FMISO within the tumor ROI.

However, there were individual cases for which the tumor hypoxia, as reflected by the 2 putative measures—that is, late T/B ratio and K_i—did not result in good intratumoral regional concordance. An example of this is shown in Figure 5, for patient 8, for whom there was an ambiguity between the high intensity voxels in the late T/B image and parametric K_i image. The T/B in the tumor ROI, as shown in Figure 5A, has moderately high intensity in a region that includes and extends beyond the tumor ROI, with average T/B = 1.36 in the larger region and T/B = 1.52 in the tumor ROI. However, only a subregion of the tumor ROI in the K_i image appeared to be hypoxic. The average K_i in this subregion was 0.0020 (1/min) and in the tumor

ROI was 0.0013 (1/min). The tumor ROI time–activity curve flats out at a late time in the tumor subregion, as shown in Figure 5B.

Correlation of Tumor Hypoxia, Local Blood Perfusion, and Local Vasculature Distribution

For these 9 patients and over the tumor ROI, the correlation coefficent between the average surrogate perfusion rate constant k_1 and the average hypoxia retention rate constant K_i was −0.33 (slight negative correlation), between the average vascular volume fraction β and average K_i it was 0.54 (moderate positive correlation), and between the average β and average k_1 it was −0.08 (no correlation).

Threshold to Identify Tumor Hypoxia

The existence of a good correlation between average T/B and K_i in tumor ROI raises the question of whether there is any threshold to identify hypoxia based on a (T/B, K_i) scatter plot. To investigate this, 2 (T/B, K_i) scatter plots were created for individual voxels within the tumor ROI and all voxels within the entire head and neck field of view. Figure 6 displays the scatter plots for patients 2 (top row), 9 (middle row), and 8 (bottom row). The left column is the scatter plot for the whole head and neck region (including the tumor ROI). The center column is the scatter plot for voxels corresponding to the tumor ROI only. The scatter plot in the right column is for all of the voxels within the entire head and neck region, but in which the intratumor voxels representing predicted tumor hypoxia are displayed as red triangles and tumor normoxia is represented by the green squares.

For patient 2 (top row), there appears to be significant hypoxia within the whole tumor ROI volume. From Figure 6 (top left), we see that most normoxic tissues lie in the lower left corner of the scatter plot, where dotted points are clustered densely together, with T/B less than 1.6 and K_i less than 0.00275. The hypoxic tumor ROI values lie in the upper-right corner where the sparse points are, as shown in Figure 6 (top center and top right), where most K_i are greater than 0.00275 and most triangles lie above the red dashed linear regression line. Therefore, for this patient, the hypoxic tumor region can be well separated from the normoxic normal tissues.

Patient 9 is shown in the middle row, where the whole tumor ROI is normoxic (no hypoxia). The whole head and neck region was densely clustered together. As shown in Figure 6 (middle left), most T/B are less than 1.4 and K_i is less than 0.00225, and there are almost no sparsely clustered regions. The tumor ROI values lie in the lower right corner of the scatter plot, as shown in Figure 6 (middle center and middle right), and right below the dashed linear regression line.

Patient 8 is shown in the bottom row, where only a subtumor region is predicted to be hypoxic based on the parametric image data (Fig. 5). The whole head and neck region is densely clustered together in the lower left corner, with most T/B less than 1.4 and K_i less than 0.002, as shown in Figure 6 (bottom left). The whole tumor ROI has a T/B greater than 1.3 and is divided into 2 subregions by the linear regression line, as shown in Figure 6 (bottom center and bottom right). The subtumor region that is hypoxic (shown with red triangles) is above the linear regression line, and the subregion that is normoxic (shown with green squares) is mostly below the linear regression line. From these 3 examples, we can deduce that using T/B alone may not be an adequate threshold to identify hypoxia. Instead, we propose that using the (T/B, K_i) scatter plot in combination with K_i and linear regression line results in a more robust criterion.

DISCUSSION

Imaging patients at a single late time point after injection is simple and convenient for both clinical staff and the patients. Furthermore, it follows the paradigm of other routine nuclear imaging protocols such as ^{18}F-FDG PET, where the time selected for imaging after injection considers the balance between competing factors such as tumor uptake, clearance from blood, and count statistics of a decaying radioisotope. For ^{18}F-FMISO PET, it is necessary to image the patients at least 2.5 h after injection, because of the slow improvement (rise) in contrast between hypoxic and normoxic tissue. For ^{18}F-labeled hypoxia tracers, count statistics are of concern because of the necessity of late-time-point imaging, if images representing tumor hypoxia are to be achieved. As a consequence, fluctuations in the individual intratumor voxel intensities can affect the interpretation of which voxels are considered positive versus negative when threshold values are assigned to define regional hypoxia.

In this study, we observed a positive correlation (0.86) between the ROI T/B and the average K_i for that ROI, a potential hypoxia measurement for the tumor. However, because of the statistical photon counting noise in PET and the amplification of noise in kinetic analysis, the direct voxel-to-voxel correlation between T/B and K_i serving as a hypoxia index is not obvious. In addition to the statistical fluctuations for each voxel over time, there are registration uncertainties of about 1 CT voxel between the 3 separate images segments from 0 to 30, 90 to 100, and 180 to 190 min. This degree of registration accuracy can be achieved when patients are immobilized in a head-and-shoulder immobilization mask (24) but would incur larger errors for tumors at other sites (except the brain) of the body. A simulation study to investigate the effect of different errors on the resultant parameter estimation, accuracy, and precision on voxel-based compartmental analysis has been published by our group (18).

In terms of tumor ROI, there is only a slight negative correlation between surrogate perfusion rate k_1 and tumor hypoxia measure K_i (−0.33), a moderate positive correlation of vascular volume fraction β and K_i (0.54), but no correlation between β and k_1 (−0.08). The slight negative correlation between perfusion and tumor hypoxia represented by the surrogate parameters k_1 and K_i, respectively, is consistent with findings in studies by Gagel et al. (11) and Thorwarth et al. (17). However, these correlation studies need to be repeated on a larger group of patients to have any statistical significance. We also need to correlate the hypoxia, perfusion, and vascular volume fraction with treatment outcome with a larger population of patients.

The analysis performed in our study is from a pilot study consisting of 9 head and neck patients. Although small, the results of our study concur with the findings reported by Thorwarth et al. (17) that a single T/B threshold in the late-time ^{18}F-FMISO image may not be adequate and sufficient to represent the spatial distribution of hypoxia within tumors. This may be inconvenient for those seeking a simple PET procedure of inject, wait, and scan with which to identify tumor hypoxia. The clearance of ^{18}F-FMISO from highly perfused tissue may result in T/B values comparable to the low-level trapping of ^{18}F-FMISO in hypoxic regions at the 1.5- to 3-h time of PET after injection. Later imaging times can result in significant image noise and variation in voxelized T/B. The consequence of this is that voxel-based subregional analysis of tumors may exhibit high T/B but with low K_i, leading to the ambiguity between the 2 potential surrogate PET measures of tumor hypoxia observed in this study. Potential errors, resulting from the misinterpretation of such regions, can be overcome if a composite criterion, which includes the additional use of a parametric hypoxia measure such as (T/B, K_i), is used to identify regional tumor hypoxia. Most hypoxic tumor voxels, when defined by this dual metric, are likely to locate at the sparse region of the (T/B, K_i) scatter plot, separated from the normal tissue cluster region, at a high K_i value and above the linear regression line. This (T/B, K_i) clustering technique might be useful to define biologic target volume in radiotherapy for functional image-based dose escalation.

The focus of this study was to investigate the potential of k_3, K_i, and late-time-point T/B as voxelized image maps as surrogate measures for the intratumor distribution of hypoxia. There were also other potential surrogate measures of tumor hypoxia, such as k_1/k_2, that were calculated (Table 1) but not further discussed in this article.

CONCLUSION

Different surrogate measures of intratumor hypoxia may be good concordance for a fraction of patients, but ambiguities can arise, in particular between the measures obtained by compartmental analysis (k_3 and K_i) and simple T/B from late-time-point imaging. The parametric image maps derived in this work are not at this point proven surrogate measures of hypoxia but rather are a fit of the trapping rate constants, based on a compartmental model of ^{18}F-FMISO binding to a hypoxia compartment within the tumor tissue. The results of our analysis need to be validated against independent and more direct techniques such as image-guided partial oxygen pressure (pO_2) probe measurement or immunohistochemisty. This pilot study did not include clinical pO_2 measurements or tumor biopsy. It is part of our future plans to conduct such validation measurements in experiments performed in an animal tumor model.

Acknowledgments

This work is supported in part by NIH PO1 CA115675.

References

1. Höckel M, Knoop C, Schlenger K, et al. Intratumoral pO2 predicts survival in advanced cancer of the uterine cervix. Radiother Oncol 1993;26:45–50. [PubMed: 8438086]
2. Brizel DM, Scully SP, Harrelson JM, et al. Tumor oxygenation predicts for the likelihood of distant metastases in human whole-body sarcoma. Cancer Res 1996;56:941–943. [PubMed: 8640781]
3. Movsas B, Chapman JD, Hanlon AL, et al. Hypoxic prostate/muscle pO2 ratio predicts for biochemical failure in patients with prostate cancer: preliminary findings. Urology 2002;60:634–639. [PubMed: 12385924]
4. Nordsmark M, Overgaard M, Overgaard J. Pretreatment oxygenation predicts radiation response in advanced squamous cell carcinoma of the head-and-neck. Radiother Oncol 1996;41:31–39. [PubMed: 8961365]
5. Brizel DM, Sibley GS, Prosnitz LR, et al. Tumor hypoxia adversely affects the prognosis of carcinoma of the head-and-neck. Int J Radiat Oncol Biol Phys 1997;38:285–289. [PubMed: 9226314]
6. Stadler P, Becker A, Feldmann HJ, et al. Influence of the hypoxic subvolume on the survival of patients with head-and-neck cancer. Int J Radiat Oncol Biol Phys 1999;44:749–754. [PubMed: 10386631]
7. Nordsmark M, Bentzen SM, Rudat V, et al. Prognostic value of tumor oxygenation in 397 head-and-neck tumors after primary radiation therapy: an international multi-center study. Radiother Oncol 2005;77:18–24. [PubMed: 16098619]
8. Valk PE, Mathis CA, Prados MD, et al. Hypoxia in human gliomas: demonstration by PET with fluorine-18-fluroromisonidazole. J Nucl Med 1992;33:2133–2137. [PubMed: 1334136]
9. Rasey JS, Koh WJ, Evans ML, et al. Quantifying regional hypoxia in human tumors with positron emission tomography of [^{18}F]fluoromisonidazole: a pre-therapy study of 37 patients. Int J Radiat Oncol Biol Phys 1996;36:417–428. [PubMed: 8892467]
10. Eschmann SM, Paulsen F, Bedeshem C, et al. Hypoxia-imaging with ^{18}F-misonidazole and PET: changes of kinetics during radiotherapy of head-and-neck cancer. Radiother Oncol 2007;83:406–410. [PubMed: 17543402]
11. Gagel B, Piroth M, Pinkawa M, et al. pO2 polarography, contrast enhanced color duplex sonography (CDS), [^{18}F] fluoromisonidazole and [^{18}F] fluorodeoxyglucose positron emission tomography: validated methods for the evaluation of therapy-relevant tumor oxygenation or only bricks in the puzzle of tumor hypoxia [abstract]? BMC Cancer 2007;7:113. [PubMed: 17598907]

12. Chapman JD, Lee J, Meeker BE. Keynote address: cellular reduction of nitroimidazole drugs: potential for selective chemotherapy and diagnosis of hypoxic cells. Int J Radiat Oncol Biol Phys 1989;16:911–917. [PubMed: 2649465]

13. Casciari J, Graham MM, Rasey JS. A modeling approach for quantifying tumor hypoxia with [F-18] fluoromisonidazole PET time-activity data. Med Phys 1995;22:1127–1139. [PubMed: 7565388]

14. Rajendran JG, Mankoff DA, O'Sullivan F, et al. Hypoxia and glucose metabolism in malignant tumors: evaluation by [^{18}F]fluoromisonidazole and [^{18}F]fluorodeoxyglucose positron emission tomography imaging. Clin Cancer Res 2004;10:2245–2252. [PubMed: 15073099]

15. Rajendran JG, Schwartz DL, O'Sullivan J, et al. Tumor hypoxia imaging with [F-18] fluoromisonidazole positron emission tomography in head and neck cancer. Clin Cancer Res 2006;12:5435–5441. [PubMed: 17000677]

16. Thorwarth D, Eschmann SM, Paulsen F, et al. A kinetic model for dynamic [^{18}F]-Fmiso PET data to analyze tumor hypoxia. Phys Med Biol 2005;50:2209–2224. [PubMed: 15876662]

17. Thorwarth D, Eschmann SM, Scheiderbauer J, et al. Kinetic analysis of dynamic ^{18}F-fluoromisonidazole PET correlates with radiation treatment outcome in head-and-neck cancer [abstract]. BMC Cancer 2005;5:152. [PubMed: 16321146]

18. Wang W, Georgi J-C, Nehmeh SA, et al. Evaluation of compartmental model for estimating tumor hypoxia via FMISO dynamic PET imaging. Phys Med Biol 2009;54:3083–3099. [PubMed: 19420418]

19. Huang, SC.; Phelps, ME. Principles of tracer kinetic modeling in positron emission tomography and autoradiography. Phelps, M.; Mazziotta, J.; Schelbert, H., editors. New York: Raven Press; 1986. p. 287-345.

20. Wahl RL, Zasadny K, Helvie, Hutchins GD, Weber B, Cody R. Metabolic monitoring of breast cancer chemohormonotherapy using positron emission tomography: initial evaluation. J Clin Oncol 1993;11:2101–2111. [PubMed: 8229124]

21. Gupta N, Gill H, Graeber G, et al. Dynamic positron emission tomography with F-18 fluorodeoxyglucose imaging in differentiation of benign from malignant lung/mediastinal lesions. Chest 1998;114:1105–1111. [PubMed: 9792584]

22. Hoekstra CJ, Hoekstra OS, Lammertsma AA. On the use of image-derived input functions in oncological fluorine-18 fluorodeoxyglucose positron emission tomography studies. Eur J Nucl Med 1999;26:1489–1492. [PubMed: 10552093]

23. Jensen-Urstad K, Jensen-Urstad M, Johansson J. Carotid artery diameter correlates with risk factors for cardiovascular disease in a population of 55-year-old subjects. Stroke 1999;30:1572–1576. [PubMed: 10436103]

24. Hong TS, Tomé WA, Chappell RJ, et al. The impact of daily setup variations on head-and-neck intensity-modulated radiation therapy. Int J Radiat Oncol Biol Phys 2005;61:779–788. [PubMed: 15708257]

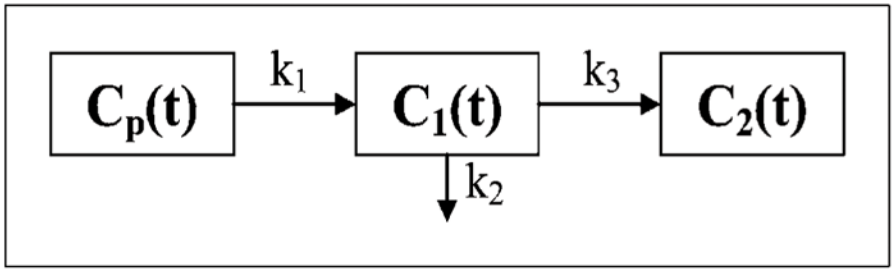

FIGURE 1.
Generic irreversible 1-plasma, 2-tissue compartmental model.

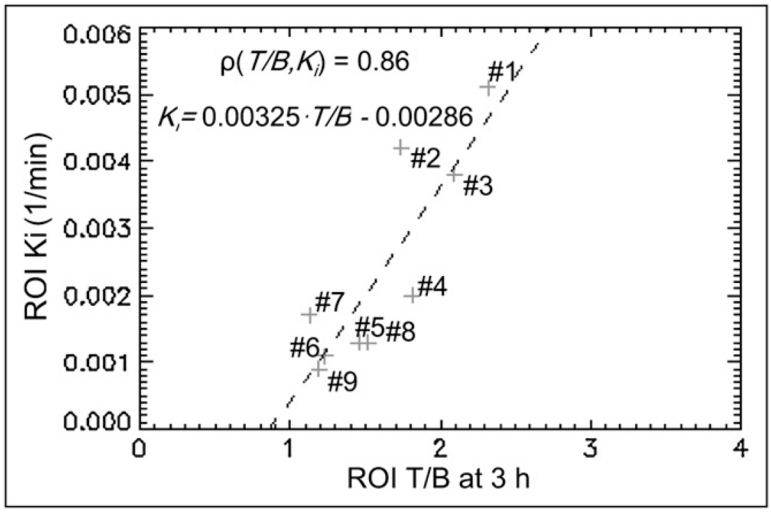

FIGURE 2.
Scatter plot of average (T/B, K_i) in tumor ROI for 9 patients.

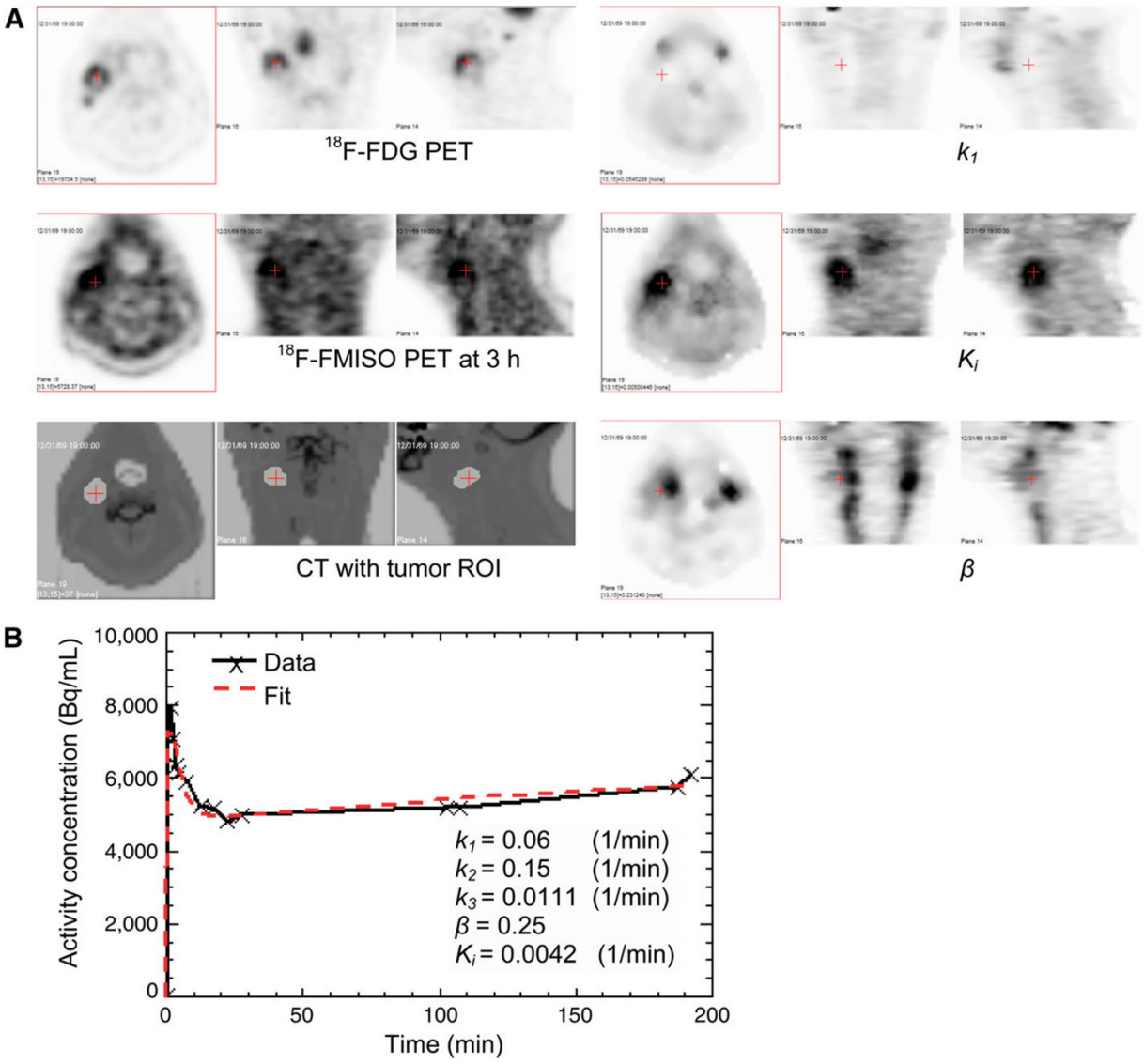

FIGURE 3.

Concordance between high values of parametric hypoxia index K_i and high T/B in late-time image for patient 2. Transverse, coronal, and sagittal views are shown for ^{18}F-FDG PET, ^{18}F-FMISO PET at 3 h, CT fused with tumor ROI, k_1, K_i, and β (A) and measured and fitted average activity concentration in tumor ROI as function of time (B).

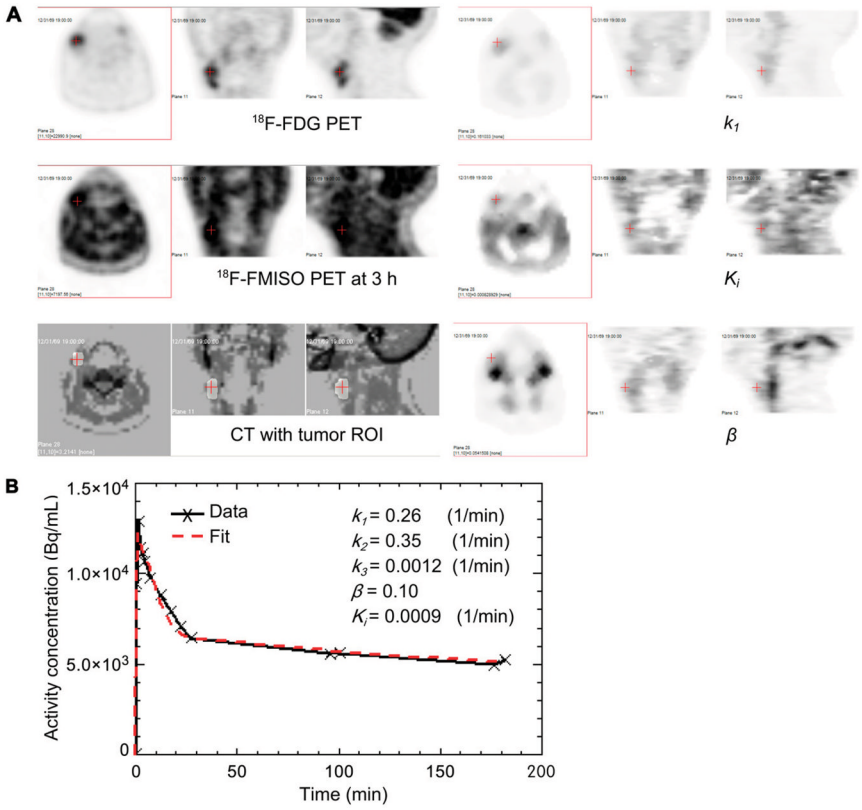

FIGURE 4.

Concordance between parametric K_i values suspected to exhibit no or low level of tumor hypoxia and low T/B in late-time image for patient 9. Transverse, coronal, and sagittal views are shown for ^{18}F-FDG PET, ^{18}F-FMISO PET at 3 h, CT fused with tumor ROI, k_1, K_i, and β (A) and measured and fitted average activity concentration in tumor ROI as function of time (B).

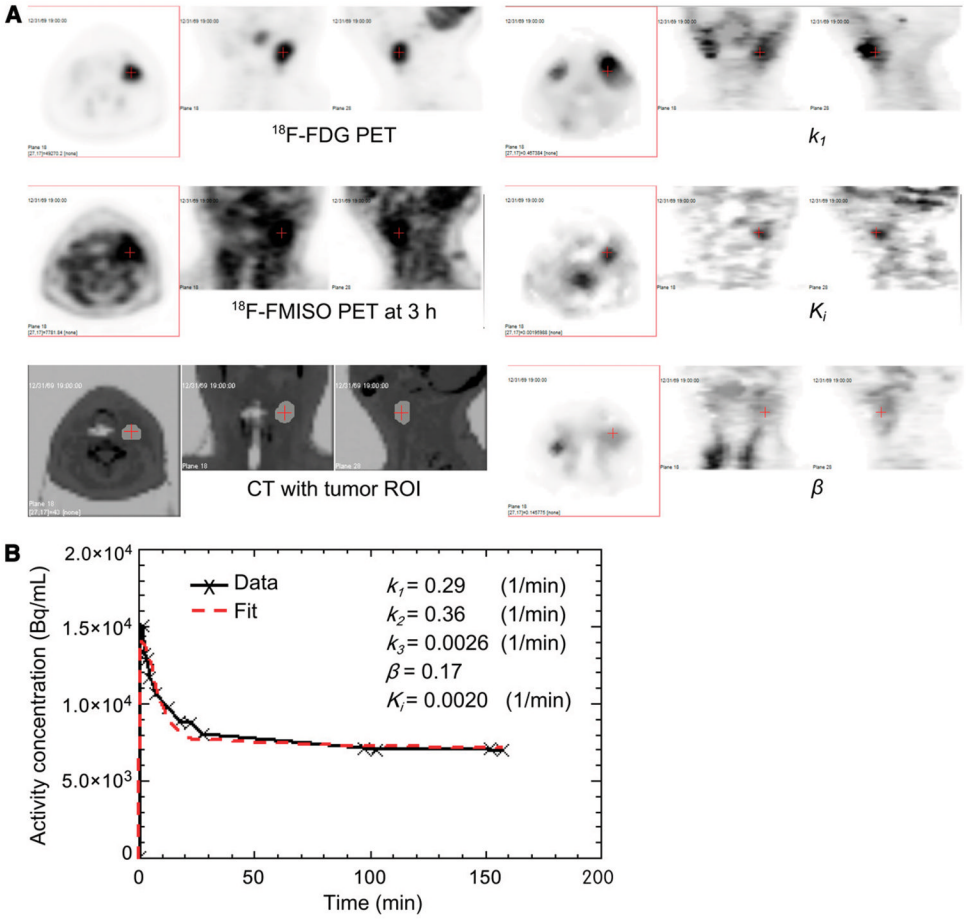

FIGURE 5.

Ambiguity in concordance between 2 surrogate measures of tumor hypoxia K_i and T/B from late-time-point imaging for patient 8. Transverse, coronal, and sagittal views are shown for ^{18}F-FDG PET, ^{18}F-FMISO PET at 3 h, CT fused with tumor ROI, k_1, K_i, and β (A) and measured and fitted average activity concentration in tumor sub-ROI as function of time (B).

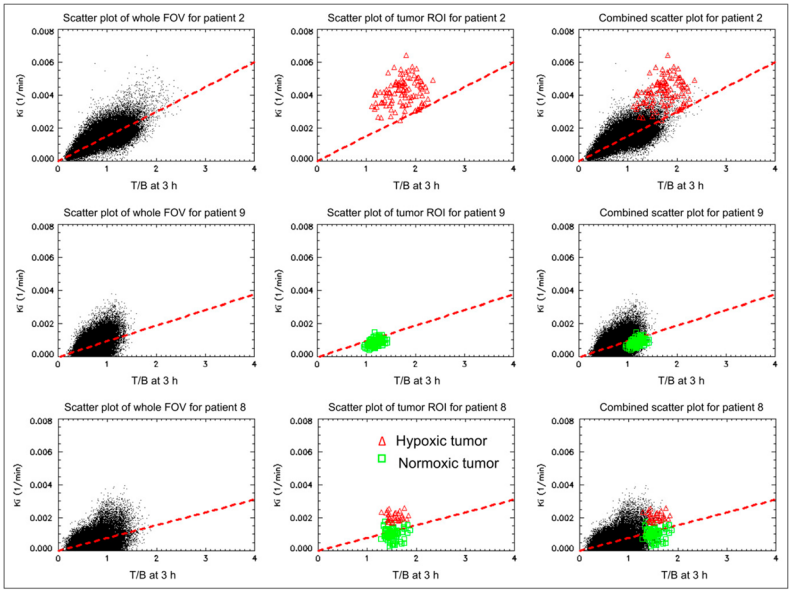

FIGURE 6.

Scatter plots of individual voxels (T/B, K_i) at both whole head and neck region and tumor ROI for patients 2 (top row), 9 (middle row), and 8 (bottom row). Whole head and neck region is shown on left, tumor ROI in center, and both regions on right. ● = whole head and neck region; red triangles = putative hypoxic tumor region; green squares = putative normoxic tumor region.

TABLE 1

Summary of Kinetic Analysis of ^{18}F-FMISO PET in Head and Neck Patients with Squamous Cell Carcinoma

Patient no.	Tumor stage	Tumor site	Tumor ROI (voxels)	ROI β	ROI k_1 (/1 min)	ROI K_i (1/min)	ROI k_1/k_2	ROI k_3 (1/min)	ROI T/B at 3 h	Tumor noise at 3 h	Input function peak/tail
1	T1N3M0	Pharyngeal	267	0.27	0.19	0.0051	0.65	0.0081	2.32	16%	9.3
2	T3N2M0	Right tonsil	112	0.25	0.06	0.0042	0.42	0.011	1.74	17%	7.3
3	T3N1M0	Right base of tongue	205	0.16	0.30	0.0038	0.86	0.0045	2.09	14%	12.0
4	T4N1M0	Base of tongue	103	0.05	0.16	0.0020	0.94	0.0022	1.81	17%	9.2
5	T2N2M0	Right tonsil	94	0.25	0.39	0.0013	0.85	0.0016	1.46	7%	8.3
6	T1N1M0	Larynx	42	0.15	0.08	0.0011	0.44	0.0026	1.23	11%	6.8
7	T3N2M0	Right pyriform sinus	238	0.04	0.31	0.0017	0.61	0.0031	1.13	9%	4.9
8	T2N2M0	Left base of tongue	114	0.17	0.32	0.0013	0.80	0.0016	1.52	9%	9.4
9	T1N2M0	Right base of tongue	89	0.10	0.26	0.0009	0.73	0.0013	1.19	10%	9.0